Research Square

Preprints are preliminary reports that have not undergone peer review.
They should not be considered conclusive, used to inform clinical practice,
or referenced by the media as validated information.

STK33 is required for the differentiation of spermatocytes and spermatids in male mice by maintaining mitochondrial homeostasis

Weiyang Zhang
Cancer Hospital Affiliated to Shanxi Medical University
Zhiyuan An
Cancer Hospital Affiliated to Shanxi Medical University
Congqiao Zhang
Cancer Hospital Affiliated to Shanxi Medical University
Qing Tian
Gaoping People's Hospital
Yangyi Wang
Hong Kong Metropolitan University
Xueqing Li
Second Hospital of Shanxi Medical University
Pan Tian
Cancer Hospital Affiliated to Shanxi Medical University
Neng Wan
Cancer Hospital Affiliated to Shanxi Medical University
Yuxing Yuan
Cancer Hospital Affiliated to Shanxi Medical University
Junying Yuan
Cancer Hospital Affiliated to Shanxi Medical University
Juan Du
Cancer Hospital Affiliated to Shanxi Medical University
Xiang Huang
Shanxi Women and Children Health Hospital
Yanling Yu
Cancer Hospital Affiliated to Shanxi Medical University
Laifeng Ren
rlaifeng@163.com

Cancer Hospital Affiliated to Shanxi Medical University

Article

Keywords: STK33, Spermatogenesis, Metabolic, Apoptosis

Posted Date: June 13th, 2026

DOI: https://doi.org/10.21203/rs.3.rs-9745803/v1

License: This work is licensed under a Creative Commons Attribution 4.0 International License.
Read Full License

Additional Declarations: No competing interests reported.

Abstract

Spermatogenesis is a highly intricate and tightly regulated cell development process, involving mitosis, meiosis and spermiogenesis. STK33, a member of the serine/threonine kinase family, is prominently expressed in testicular tissue, particularly in spermatocytes. In male mice, STK33 is essential for the spermatid differentiation and male infertility. However, the role of STK33 in spermatocyte cell development in males has remained unexplored. To further elucidate the exact role of STK33 in mouse reproduction, we generated *STK33*$^{-/-}$ mice using CRISPR/Cas9 technology. Deletion of *STK33* resulted in complete infertility in male mice, and *STK33*$^{-/-}$ mice displayed reduced sperm count compared to wild-type (WT) mice. Single-cell cytometry results of testes show that the differences between *STK33*$^{-/-}$ and WT mice mainly concentrate at the spermatocyte stage, with differentially expressed genes primarily focusing on metabolic pathways. *STK33*$^{-/-}$ mice manifested mitochondrial abnormalities and heightened apoptosis compared to WT mice. Furthermore, there were notable irregularities in the expression of proteins associated with apoptosis and mitochondrial function.In conclusion, our findings unveil a novel role for *STK33* in germ cell development in male mice, whereby knockout of the STK33 gene leads to disruption of mitochondrial homeostasis and increased cell apoptosis in mouse spermatocytes and spermtids.

Introduction

Spermatogenesis is a complex and intricately regulated process. The seminiferous tubules comprise somatic cells (Sertoli cells) and germ cells. Spermatogonia undergo mitotic division, meiosis, and spermiogenesis to generate sperm[1]. Spermatids undergo additional developmental stages, including acrosome formation, flagella assembly, histone replacement, chromatin condensation, and elimination of residual bodies to achieve maturation[2]. This process culminates in the generation of a substantial quantity of sperm that enter the epididymis[3].

Mitochondria play a crucial role in sperm development. For example, reactive oxygen species(ROS) from mitochondria act as signaling molecules or protein oxidation modifiers to regulate transcription and protein activity[4]. Mitochondrial morphology, size, and localization also change markedly in spermatogensis. Some studies suggest that the interaction between ROS and oxygen determines the self-renewal efficiency of spermatogonial stem cells(SSCs) under hypoxic conditions[5, 6]. However, excessive ROS will overwhelm the cellular antioxidant capacity and trigger apoptosis, ultimately resulting in infertility[7].

STK33 is a serine/threonine kinase that is specifically expressed in spermatocyte and elongated sperm cells. The human*STK33* gene is located on chromosome 11, specifically in the 11p11.2 region, and encodes a protein of 514 amino acids[8, 9]. Deficiency of *STK33* can lead to asthenozoospermia, inducing malformed and immotile spermatozoa[10, 11]. Recent research has shown that STK33 affects the assembly of sperm flagella through the phosphorylation of fibrous sheath proteins AKAP4/AKAP3[12]. Additionally, studies have indicated that the loss of *STK33* enhances the

mitochondrial pathway of apoptosis in cochlear cells and cancer cells[13,14]. In conclusion, further research is needed to elucidate whether STK33 which was highly expressed in spermatocyte cells plays a role in spermatocyte development and whether it functions in maintaining mitochondrial homeostasis to prevent cell apoptosis in the development of germ cells.

In this study, we generated a *STK33* knockout (*STK33*$^{-/-}$) mouse model. We observed that *STK33*$^{-/-}$ mice exhibited infertility, with a significant decrease in sperm count and noticeable morphological abnormalities. Enhanced apoptosis was detected in the testes of *STK33*$^{-/-}$ mice. Furthermore, scRNA-seq analysis revealed the spermatocyte subtypes and metabolic pathway disparities between *STK33*$^{-/-}$ and WT mice. We also detected increased ROS levels, reduced ATP levels and mitochondrial membrane potential (JC-1) in the testes of *STK33*$^{-/-}$ mice. STK33 is essential for both spermatocyte and spermatid development in male mice by maintaining mitochondrial homeostasis.

Results

STK33 exhibits specific expression in particular stages of male germ cells

By constructing an evolutionary tree and conducting homology analysis of the kinase domain, it has been revealed that STK33 is a serine/threonine kinase with a high degree of conservation (Fig.1A-B).To compare the expression patterns of STK33 in different organs between mice and humans, the highest levels of *STK33* mRNA expression were detected in the testes among various organs in mice (Fig. 1C). Subsequently, scRNA-seq was conducted on mouse testes, revealing the expression of *STK33* in spermatocytes and round spermatids (Fig. 1D). Furthermore, immunofluorescence staining performed on human testis sections confirmed the expression of STK33 in spermatocytes and round spermatid cells (Fig. 1E), consistent with the findings from scRNA-seq.

STK33 deletion leads to male infertility in mice

Previous studies have demonstrated the essential role of STK33 in spermatogenesis in mice, with its deficiency leading to infertility in this species. Clinical cases supporting these findings have also been reported. To further elucidate the function of STK33 in mouse spermatogenesis, CRISPR/CAS9 technology was employed to generate *STK33* knockout mice, targeting exons 4-7 (Fig. 2A). QPCR analysis confirmed the exclusive expression of *STK33* in wild-type (WT) mice (Supplementary Fig. 1A), indicating successful knockout of STK33 protein in *STK33*$^{-/-}$ mice.Genotyping results in the F2 generation mice displayed Mendelian inheritance (Supplementary Fig. 1B). While *STK33*$^{-/-}$ mice exhibited normal growth and health, they displayed complete infertility (Fig. 2B). The testis weight-to-body weight ratio in 12-week-old mice showed no significant difference compared to the WT group ($P>0.05$), but exhibited a higher standard deviation than the WT group (Fig. 2C). Conversely, the epididymis-to-body weight ratio was lower than that of the WT group (Fig. 2D). Furthermore, the number of sperm in the bilateral epididymis was significantly reduced in the *STK33*$^{-/-}$ group compared to the WT group (Fig. 2E).

Deletion of *STK33* results in a reduction in sperm quantity and abnormal morphology

To further investigate the underlying cause of infertility in mice resulting from *STK33* knockout, we conducted a comparative analysis of HE staining of testes from 12-week-old *STK33*$^{-/-}$ and WT mice. Our findings revealed significant morphological abnormalities in elongating spermatids in *STK33*$^{-/-}$ mice (Fig. 3A). Additionally, HE staining of the epididymis demonstrated a notable decrease in mature sperm count in *STK33*$^{-/-}$ mice (Figure 3B). Diff-quick staining of sperm indicated abnormal tail structures (Fig. 3C). Relative sperm counting results showed a decline in sperm count starting from the 14th step of development (Fig. 3E), with a more pronounced decrease observed at the 16th step (Fig. 3D-E).

Single-cell sequencing analysis revealed that the differentially expressed genes in spermatocytes and spermatids are enriched in metabolic pathways.

To investigate the molecular changes in spermatogenic cells in *STK33*$^{-/-}$ mice, scRNA-seq was performed on both *STK33*$^{-/-}$ and WT mice. After filtering, a total of 18,120 cell nuclei were obtained and analyzed using the nuclear extraction method. Subsequent dimensionality reduction clustering classified these nuclei into 28 clusters (Fig. 4A), with 20 clusters identified as spermatogenic cells. Analysis of marker gene expression generated a dimensionality reduction plot (UMAP) illustrating cell types (Fig. 4B). Further KEGG pathway enrichment analysis revealed that the differentially expressed genes between spermatocytes and spermatids were predominantly enriched in metabolic pathways(Fig. 4C-D).

Subclustering of SPC reveals significant effects of *STK33* on metabolic pathways

To further investigate the impact of *STK33* knockout on spermatocyte, we subtyped the scRNA-seq data of spermatocyte (Fig. 5A). Based on the characteristic genes of mouse testicular spermatocytes at each stage[15], SPCs were classified into nine categories based on the expression of marker genes (Fig. 5A-B). The proportion of different cell categories showed a decreased number of SPCs mainly concentrated in the late pachytene and zygotene stages, with increased numbers of cells in the diplotene and meiosis II stages as well (Fig. 5C). Further analysis of STK33 expression in subcategories of SPCs revealed that its expression was highest in the diplotene and meiosis II stages (Fig. 5D). KEGG enrichment analysis revealed that the differential gene expression between zygotene and late pachytene stage spermatocytes was concentrated in metabolic pathways (Fig. 5E-F), while diplotene and meiosis II stage spermatocytes also showed enrichment in metabolic pathways (Supplementary Fig. 2A-B).

***STK33*$^{-/-}$ mice exhibit increased apoptosis of germ cells and concomitant mitochondrial disregulation**

Terminal deoxynucleotidyl transferase-mediated dUTP nick-end labeling (TUNEL) staining was performed, revealing stronger TUNEL staining signals in the testes of *STK33*$^{-/-}$ mice, particularly in elongated spermatids and spermatocytes at stage IX-X and stage XI-XII (Fig. 6A). Our scRNA-seq data and immunofluorescence analysis demonstrated an upregulation in the expression of the DNA double strand break genes(Supplementary Fig.3A-B).To explore the potential relationship between mitochondrial metabolism and germ cell apoptosis in *STK33*$^{-/-}$ mice, ATP levels were measured in

testicular lysates. ATP levels in testicular lysates from WT mice were significantly higher than those in *STK33*$^{-/-}$ mice (Fig. 6B). Our scRNA-seq data revealed upregulation of prkag2 expression (Supplementary Fig.3A).Immunofluorescence analysis further verified an elevation in AMPK phosphorylation (Supplementary Fig.3C), indirectly supporting a reduction in ATP production[16]. Additionally, reactive oxygen species (ROS) and mitochondrial membrane potential (JC-1) were assessed in single-cell suspensions from mouse testes. ROS staining indicated elevated ROS levels in germ cells of *STK33*$^{-/-}$ mice compared to WT mice (Fig. 6C). The percentage of germ cells with high mitochondrial membrane potential was higher in WT mice than in *STK33*$^{-/-}$ mice (Fig. 6D-E).

Furthermore, electron microscopy examination of mouse testes revealed abnormal morphology and arrangement of mitochondria in *STK33*$^{-/-}$ mice compared to WT mice (Fig. 6F).The main manifestations of abnormal mitochondrial morphology are swelling and disappearance of mitochondrial cristae.

***STK33* deficiency causes transcription dysregulation of genes related to mitochondrial functions**

To further elucidate the mechanism by which STK33 affects spermatogenesis through regulating mitochondrial homeostasis, combined with the previous experimental results, we analyzed the differentially expressed genes of mitochondrial oxidative phosphorylation from the single - cell RNA sequencing data (Supplementary Fig4). We selected several representative genes generated a heatmap illustrating their gene expression (Fig. 7A).The scRNA-seq results revealed a upregulated expression of pyrophosphatase (*Ppa2*) in SPC (Fig.7B), consistent with our immunofluorescence findings. The scRNA-seq results and RNA fish indicated the expression of testis-specific cytochrome C (*Cyct*)was downregulated in SPC, spermtids, elongating, and other cell types (Fig.7C) and cytochrome c oxidase (*COX10*)was downregulated in SPG and Sertoli cells (Fig.7D). These findings were subsequently validated by our in situ hybridization probes. scRNA-seqAberrant transcription of these genes may be a significant factor in the induction of mitochondrial dysfunction by *STK33* deletion.

Discussion

Based on our findings, STK33 is a highly conserved protein throughout evolution. It is prominently expressed in mouse spermatocytes and certain germ cells, suggesting a crucial role in spermatogenesis[11]. Deletion of *STK33* results in complete infertility in male mice. Studies have demonstrated that the absence of *STK33* leads to abnormal phosphorylation of the AKAP3/AKAP4 substrate, causing sperm morphological irregularities[12]. Additionally, *STK33* knockout in mice results in a notable reduction in sperm count and an increase in apoptosis. This suggests that STK33 may affect not only the sperm shaping stage.

In the results of HE staining, We observed a significant decrease in elongating spermatids at the final stage of development, as well as a substantial reduction in mature sperm stage. We speculate that sperm development is arrested at late elongating spermatids stage. scRNA-seq data showed that spermatocyte exhibited the greatest differential expression among cell types. This may suggest that the

deletion of STK33 results in significant differences at the spermatocyte stage. Subclassification of spermatocyte revealed a reduction primarily in late pachytene and zygotene spermatocytes. Conversely, there was a noticeable increase in the proportion of spermatocytes at the diplotene and meiosis II stages in *STK33*$^{-/-}$ mice. Further analysis indicated that the abnormal expression of genes in late pachytene, diplotene, zygotene, and meiosis II stages mainly involved metabolic pathways rather than meiosis pathways. This suggests that cell division during the diplotene stage and meiosis II may be arrested due to metabolic abnormalities.ScRNA-seq data indicates that the differentially expressed genes between the two groups are predominantly enriched in metabolic pathways. Mitochondrial function is closely intertwined with sperm development and apoptosis[18, 19]. Our investigation reveals that *STK33* deficiency leads to a decrease in mitochondrial membrane potential, an increase in reactive oxygen species, and a decline in ATP levels[20-22]. Dysfunctional mitochondria may trigger apoptosis[23, 24]. Electron microscopy observations display disordered mitochondrial arrangement and blurred cristae in *STK33*$^{-/-}$ mice, confirming aberrant mitochondrial function[25].

Through further scrutiny of scRNA-seq outcomes, we observed heightened expression of apoptosis-related proteins and distorted expression of mitochondrial-related proteins following *STK33* knockout. Aging-related proteins P70 and Ki67 exhibited no significant differences compared to the wild type, suggesting that mitochondrial dysfunction is not aging-related[26, 27]. COX10 protein, a pivotal mitochondrial protein, primarily serves as an assembly factor for the cytochrome c oxidase (COX) complex[28]. Cyct is a testis-specific cytochrome C[29]. We postulate that the downregulation of Cyct is associated with abnormal mitochondrial function, while the upregulation of COX family proteins, represented by COX10, is a compensatory response. PPA2 indirectly participates in regulating the energy status and balance of various enzyme-catalyzed reactions by modulating the concentration equilibrium of pyrophosphate and phosphate[30]. We propose that the increase in PPA may be linked to the decrease in ATP levels.

TUNEL staining and apoptosis-related protein staining revealed that apoptosis in *STK33*$^{-/-}$ mice primarily occurred in spermatocytes. STK33 is predominantly expressed in primary spermatocytes, and the affected mitochondrial proteins in knockout mice are primarily abnormal in primary spermatocytes.

Research has demonstrated that oral administration of *STK33*-targeted inhibitors can achieve contraceptive effects, confirming the essential role of STK33 in sperm development[31]. Moreover,STK33 co-localizes with wave protein in the hypothalamus and functions as a kinase to phosphorylate wave protein[32]. Furthermore, there is evidence supporting the significant involvement of STK33 in pulmonary fibrosis[33]. Nevertheless, STK33 is not prominently expressed in brain and lung tissues; rather, it exhibits specific expression in the testes of mice.Consequently, our primary focus is to investigate the role and mechanism of STK33 in spermatogenesis.

Conclusion

In summary, our genetic sequencing and phenotype data, derived from a mouse model, suggest that the absence of *STK33* triggers apoptosis in germ cells. Our phenotype data also indicate that the deletion of *STK33* not only causes aberrant sperm morphology but also notably diminishes the quantity of mature sperm. This paper further elucidates the impact of STK33 deficiency on mitochondrial function.The impact of STK33 is not limited to the haploid cell stage, but also plays a significant role in stages such as spermatocytes. Nevertheless, the mechanisms and phosphorylation substrates linked to mitochondrial metabolism remain elusive, and this will be the primary focus of our upcoming investigations.

Materials and methods

Animals

The *STK33* KO mice were generated and maintained on C57BL/6J background using CRISPR/Cas9 technology (Cyagen Biosciences Inc., Suzhou, China).Briefly,Single guide RNAs (sgRNAs) were selected to target the entire coding area of *STK33* and were as follows:5′-ACTTGCACTAGATGGAC TACAGG-3′ and 5′-GTACAAGTCACTGGCCCATTAGG-3′ Injected plasmid Cas021Am-*STK33*-gRNA -Cas9 with gRNA was constructed. After in vitro transcription, *STK33* gRNA and cas9 mRNA were micro-injected into C57BL/6J zygotes to obtain F0 positive (8 bp) mice identified by PCR and DNA sequencing using following primers:F1: 5′-CTCAGGATCCCAAACAGTTAAGAT-3′ and R1: 5′-GTATCA CCTGACAAGGGAGAACTG-3′, fragment size of 632 bp.Mating F0 with WT mice to obtained F1 mice. F2 mice were obtained by mating heterozygous F1 litters. Heterozygous male and female mice were used for subsequent breeding and mating.Homozygous twelve-week *STK33* KO and WT (control group) male mice were used for experiments. Micewere housed in a temperature and light regulated room in a SPF facility and received food and water ad libitum. Animals were euthanized by cervical dislocation at the end of the experiment. This method was performed in accordance with the AVMA Guidelines for the Euthanasia of Animals and was approved by the Ethics Committee of Shanxi Cancer Hospital, (Approval No. [DWLL2024006]).

QPCR assays

RNA of different mouse tissues were extracted using the TRIzol reagent (Promega, LS1040). RNA samples were reverse transcripted using the RevertAid First Strand cDNA Synthesis Kit (Promega,A2791). Semi-quantitative PCR was performed under the following cycling conditions (Promega,A6001).Reaction mixture was first heated at 95°C for 3 min. 25 cycles were then carried out with the following parameters: denaturing at 95°C for 20 s, anneal ing at 60°C for 30 s, extension at 72°C for 45 s. Reaction was finished with a final extension at 72°C for 5 min.

Primers information were as follows:

β-actin-F: 5'-GTGCTATGTTGCTCTAGACTTCG-3',

β-actin-R:5'-ATGCCACAGGATTCCATACC-3',

STK33-F: 5'-ATGTCCAGCAGGCAAGTCTC-3',

STK33-R:5'-GTGACATTGCTCCGACTCCA-3'.

Diff-Quik Staining

Immerse air-dried sperm smears in methanol for 5 min; air-dry completely.

Dip slides in Solution I (eosin-based) for 5 sec; rinse gently with distilled water. Immerse in Solution II (methylene blue) for 10 sec; rinse until background clears.Air-dry vertically or use 37°C incubator for 5 min.Analyze sperm morphology under oil immersion.

TUNEL assays

Terminal deoxynucleotidyl Transferase dUTP Nick End Labeling (TUNEL) assay was carried out according to the manufacturer of DeadEnd™ Fluorometric TUNEL System kit (Promega, 0000554959). Images were captured using a confocal microscope.

Immunofluorescence staining

Fresh mouse tissues were fixed with 4% paraformaldehyde and embedded in paraffin for sectioning. Deparaffinization was performed using xylene and a gradient of ethanol. Permeabilization was achieved with 0.3% Triton X-100 for 10 minutes, followed by antigen retrieval using sodium citrate antigen retrieval solution (Beyotime, P0081) at a temperature above 100°C for 2 minutes. Blocking was carried out using goat serum and bovine serum albumin for 1 hour. The primary antibody was incubated overnight at 4°C. After three washes with PBS, the secondary antibody was incubated at 37°C for 30 minutes. Finally, the sections were counterstained with DAPI and observed under a confocal microscope.

The staining of human testicular tissue also followed the steps described above. This study was approved by the Ethics Committee of Shanghai Outdo Biotech Company (Approval No. [YBM-05-02]) , and written informed consent was obtained from all patients. The research was conducted in strict accordance with the principles of the Declaration of Helsinki. All experiments were conducted in accordance with the relevant guidelines and regulations.

ATP Determination

Spermatozoa ATP was carried out according to the manufacturer instructions of enhanced ATP assay kit (Beyotime, S0027). Briefly, fluorescein can be catalyzed to generate fluorescence by luciferase. When both fluorescein and luciferase are excessive, the production of fluorescence is proportional to the concentration of ATP within a certain concentration range of 0.1 nM to 10 mM. For 20 mg of tissue, add 100-200 μL of lysis buffer, and homogenize using a homogenizer. After lysis, centrifuge at 12,000 g for 5 minutes at 4°C Collect the supernatant for analysis.

ROS and JC-1 Determination

The specimen used fresh mouse testes, which were added to 6ml preheated (35℃) DMEM medium. Then, 12ul of collagenase (200U/ml) and 2ul of DNAse (5ug/ml) were added. The mixture was incubated at 35℃ and 150rpm for 10 minutes on a shaker, with one agitation in the middle to help disperse the tubes. After a 2-minute rest, the supernatant (containing somatic cells) was removed, leaving only the coverable liquid. Another 6ml of preheated DMEM medium was added, along with 12ul of collagenase (200U/ml), 2ul of DNAse (5ug/ml), and 60ul of 2.5% trypsin. The mixture was incubated at 35℃ and 150rpm for 10 minutes on a shaker, with an additional 60ul of 2.5% trypsin added during the digestion process. The tubes were agitated 10 times up and down, with a final agitation at the end. After digestion, 1ml of FBS was added to neutralize the trypsin, and the cell suspension was used for subsequent experimental analysis.

ROSmeasurement was carried out according to the manufacturer instructions of Reactive Oxygen Species Assay Kit (Biyotime, S0033S).After adding DCFH-DA to the cell suspension from the previous step, it was incubated in the dark for 30 minutes, followed by detection using flow cytometry.2',7'-Dichlorodihydrofluorescein diacetate (DCF-DA) fluorescence was recorded at 525 nm following sequential excitation at 480 nm and normalized to spermatozoa counts.

Mitochondrial membrane potential assay was carried out mitochondrial membrane potential assay kit with JC-1(Beyotime, C2006). Briefly, spermatozoa were incubated in JC-1 working solution for 20 min at 37 C in dark. After a centrifugation at 500 g and three washes using JC-1 buffer solution, spermatozoa pellets were resuspended for further analysis using flow cytometry according to manufacturer’s protocol.

Transmission electron microscopy

Testicular tissue samples, not exceeding 1 mm^3 in size, were primarily fixed in TEM-grade glutaraldehyde fixative at room temperature for 1 hour. Subsequently, the samples were transferred to fresh fixative in microcentrifuge tubes for continued fixation. Following fixation, the tissues were rinsed three times (15 minutes each) with 0.1 M phosphate-buffered saline (PBS, pH 7.4). Post-fixation was performed using 1% osmium tetroxide (in PBS) for 2 hours at room temperature, followed by another three washes with PBS (15 minutes each).

Dehydration was carried out through a graded ethanol series (30%, 50%, 70%, 80%, 95%, and 100% twice) for 20 minutes per step, followed by two 15-minute treatments with acetone. Tissue infiltration and embedding were then performed using EMBed 812 resin (SPI, 90529-77-4) according to the following schedule: a 1:1 mixture of acetone and resin for 2-4 hours at 37°C, followed by a 1:2 acetone:resin mixture overnight at 37°C, and finally pure resin for 5-8 hours at 37°C. The tissues were then placed in embedding molds filled with pure resin and oriented, remaining at 37°C overnight. The molds were transferred to a 65°C oven for polymerization for over 48 hours. After polymerization, the hardened resin blocks were removed from the molds and stored at room temperature.

Ultrathin sections (60-80 nm) were cut using an ultramicrotome (Leica UC7) and collected on 150-mesh copper grids coated with Formvar film. The grids were stained in the dark with 2% uranyl acetate in 50% ethanol for 8 minutes, rinsed with 70% ethanol and ultrapure water, and then counterstained with 2.6% lead citrate (protected from atmospheric CO_2) for 8 minutes, followed by thorough rinsing with ultrapure water. After drying on filter paper, the grids were stored overnight at room temperature. Ultrastructural examination and image acquisition were performed using a Hitachi HT7800 transmission electron microscope. The TEM imaging service was provided by the Guangzhou Huayin Health Group.

Single-cell sequencing

The single-cell sequencing(scRNA-seq) service in this study was provided by Lianchuan Biotechnology Company (Hangzhou, China). The method used was tissue dissociation, where cell nuclei were directly extracted from the tissue and prepared as single-cell nuclear suspensions for single-cell nuclear transcriptome sequencing. Firstly, tissue cells were extracted through tissue grinding, and the 10x genomics platform utilized microfluidic technology to isolate individual cell nuclei. Then, the nucleotide sequences (barcodes) and primers with cell nucleus labeling information, as well as individual cell nuclei, were encapsulated in droplets to form a gel bead-in-emulsion (GEMs) structure. Reverse transcription reagents were released and mRNA was released from the cell nuclei through lysis in the droplets. SMART technology was used to obtain cDNA with barcodes for sequencing. After the liquid oil layer was disrupted, the cDNA underwent subsequent library construction and was sequenced using the Illumina sequencing platform (NovaSeq 6000 or NovaSeq X). A total of 20,515 cell nuclei were obtained from two samples.

RNA in situ hybridization

Fresh testicular tissue was fixed in 4% paraformaldehyde containing 0.1% DEPC for 1 hour. After dehydration and embedding in paraffin, the tissue was sectioned into 7 μm slices for RNA fish. The experiment was carried out according to the manufacturer of Enhanced Sensitive ISH Detection kit (CY3) (Doctor's, MK1033). Probes were labeled with digoxigenin. The sections were deparaffinized, digested, and pre-hybridized, followed by overnight hybridization at 37°C. A series of signal amplification steps were performed, and the samples were observed under a fluorescence confocal microscope.

Statistics and reproducibility

Statistical analysis of data from at least three independent biological replicates for comparison were carried out using unpaired Student’s t test performed in GraphPad Prism 6.0. In figures, data are represented as means ± SEM. A value of $p < 0.05$ were considered statistically significant. (*$p < 0.05$; **$p < 0.01$; ***$p < 0.001$; ****$p < 0.0001$; ns, not significant).

Declarations

Acknowledgement

We thank the Laboratory Animal Center of Shanxi Province Cancer Hospital for mouse housing and care. We also thank the Tumor Biobank of Shanxi Province Cancer Hospital for preparation of tissueslices.

Author contributions

Y.Y., L.R., and X.H. designed cellular and zoological experiments, and W.Z., Z.A. and C.Z. carried out these experiments with the assistance of Q.T., Y.W., P.T., N.W., Y.Y., Y.Z., J.Y. and J.D. Y.Y., L.R. and X.H. supervised the overall project and wrote the manuscript with W.Z.

Fundings

This work is supported by the Shanxi Provincial Natural Science Foundation (202403021211128, and 202203021211033), Key International Science and Technology Cooperation Projects of Shanxi Province (202304041101036), Central Government Guides Local Science and Fund program for the Scientific Activities of Selected Returned Overseas Professionals in Shanxi Province (20230060).

Data Availability Statement

All the data are available in the main text or supplementary materials.

Informed Consent Statement

Not applicable.

Competing interests

The authors declare no competing interests.

Ethics approval

The biopsy and pathological paraffin-embedded specimens (human testicular tissue sections) used in this study were obtained from Shanghai Outdo Biotech Company. This study was approved by the Ethics Committee of Shanghai Outdo Biotech Company (Approval No. [YBM-05-02]) , and written informed consent was obtained from all patients. The research was conducted in strict accordance with the principles of the Declaration of Helsinki.

References

1. Nishimura H, L'Hernault SW (2017) Spermatogenesis. Curr Biol. 27(18):R988-R994. https://doi.org/10.1016/j.cub.2017.07.067
2. Meistrich ML, Hess RA (2013) Assessment of spermatogenesis through staging of seminiferous tubules. Methods Mol Biol. 927:299-307.https://doi.org/10.1007/978-1-62703-038-0_27.
3. Griswold MD (2016) Spermatogenesis: the commitment to meiosis. Physiol Rev. 96(1):1-17.https://doi.org/10.1152/physrev.00013.2015.

4. Shadel GS, Horvath TL. Mitochondrial ros signaling in organismal homeostasis. Cell. 2015;163(3):560-569.https://doi.org/10.1016/j.cell.2015.10.001
5. Morimoto H, Yamamoto T, Miyazaki T, Ogonuki N, Ogura A, Tanaka T,et al (2021) An interplay of nox1-derived ros and oxygen determines the spermatogonial stem cell self-renewal efficiency under hypoxia. Genes Dev. 35(3-4):250-260. https://doi.org/10.1101/gad.339903.120
6. Morimoto H, Kanastu-Shinohara M, Ogonuki N, et al (2019) ROS amplification drives mouse spermatogonial stem cell self-renewal. Life Sci Alliance. 2(2). https://doi.org/10.26508/lsa.201900374
7. Chen W, Sun Y, Sun Q, Zhang J, Jiang M, Chang C, et al (2020) Mfn2 plays a distinct role from mfn1 in regulating spermatogonial differentiation. Stem Cell Reports.14(5):803-817. https://doi.org/10.1016/j.stemcr.2020.03.024
8. Mujica AO, Brauksiepe B, Saaler-Reinhardt S, Reuss S, Schmidt ER (2005) Differential expression pattern of the novel serine/threonine kinase, STK33, in mice and men. FEBS J. 272(19):4884-4898. https://doi.org/10.1111/j.1742-4658.2005.04900.x
9. Mujica AO, Hankeln T, Schmidt ER (2001) A novel serine/threonine kinase gene, STK33, on human chromosome 11p15.3. Gene. 280(1-2):175-181. https://doi.org/10.1016/s0378-1119(01)00780-6
10. Ma H, Zhang B, Khan A, Zhao D, Ma A, Zhou J, et al (2021) Novel frameshift mutation in stk33 is associated with asthenozoospermia and multiple morphological abnormalities of the flagella. Hum Mol Genet. 30(21):1977-1984.https://doi.org/10.1093/hmg/ddab165
11. Martins LR, Bung RK, Koch S, Richter K, Schwarzmuller L, Terhardt D,et al (2018) Stk33 is required for spermatid differentiation and male fertility in mice. Dev Biol. 433(1):84-93.https://doi.org/10.1016/j.ydbio.2017.11.007
12. Yu W, Li Y, Chen H, et al (2023) STK33 Phosphorylates Fibrous Sheath Protein AKAP3/4 to Regulate Sperm Flagella Assembly in Spermiogenesis. Mol Cell Proteomics. 22(6):100564. https://doi.org/10.1016/j.mcpro.2023.100564
13. Zhou M, Sun G, Zhang L, Zhang G, Yang Q, Yin H, Li H, et al (2018) Stk33 alleviates gentamicin-induced ototoxicity in cochlear hair cells and house ear institute-organ of corti 1 cells.J Cell Mol Med.22(11):5286-5299.https://doi.org/10.1111/jcmm.13792
14. Scholl C, Frohling S, Dunn IF, Schinzel AC, Barbie DA, Kim SY, et al (2009) Synthetic lethal interaction between oncogenic kras dependency and stk33 suppression in human cancer cells. Cell.137(5):821-834.https://doi.org/10.1016/j.cell.2009.03.017
15. Chen Y, Zheng Y, Gao Y, et al (2018) Single-cell RNA-seq uncovers dynamic processes and critical regulators in mouse spermatogenesis. Cell Res. 28(9):879-896. https://doi.org/10.1038/s41422-018-0074-y
16. Steinberg GR, Hardie DG (2023) New insights into activation and function of the ampk. Nat Rev Mol Cell Biol. 24(4):255-272.https://doi.org/10.1038/s41580-022-00547-x
17. Caldwell AS, Middleton LJ, Jimenez M, et al (2014) Characterization of reproductive, metabolic, and endocrine features of polycystic ovary syndrome in female hyperandrogenic mouse models.

Endocrinology. 155(8):3146-3159. https://doi.org/10.1210/en.2014-1196

18. Zhao S, Heng N, Wang H, Wang H, Zhang H, Gong J, et al (2022) Mitofusins: from mitochondria to fertility. Cell Mol Life Sci. 79(7):370.https://doi.org/10.1007/s00018-022-04386-z
19. Qi B, He L, Zhao Y, Zhang L, He Y, Li J, et al (2020) Akap1 deficiency exacerbates diabetic cardiomyopathy in mice by ndufs1-mediated mitochondrial dysfunction and apoptosis. Diabetologia. 63(5):1072-1087.https://doi.org/10.1007/s00125-020-05103-w
20. Wang Y, Xi W, Zhang X, Bi X, Liu B, Zheng X, et al (2023) Ctsb promotes sepsis-induced acute kidney injury through activating mitochondrial apoptosis pathway. Front Immunol. 13:1053754.https://doi.org/10.3389/fimmu.2022.1053754
21. Harrington JS, Ryter SW, Plataki M, Price DR, Choi AMK (2023) Mitochondria in health, disease, and aging. Physiol Rev. 103(4):2349-2422. https://doi.org/10.1152/physrev.00058.2021
22. Green DR, Kroemer G (2004) The pathophysiology of mitochondrial cell death. Science. 305(5684):626-629.https://doi.org/10.1126/science.1099320
23. Burke PJ. Mitochondria, bioenergetics and apoptosis in cancer (2017)Trends Cancer. 3(12):857-870.https://doi.org/10.1016/j.trecan.2017.10.006
24. Abate M, Festa A, Falco M, Lombardi A, Luce A, Grimaldi A, et al (2020) Mitochondria as playmakers of apoptosis, autophagy and senescence. Semin Cell Dev Biol. 98:139-153.https://doi.org/10.1016/j.semcdb.2019.05.022
25. Kuang W, Zhang J, Lan Z, et al (2021) SLC22A14 is a mitochondrial riboflavin transporter required for sperm oxiative phosphorylation and male fertility. Cell Rep. 35(3):109025.https://doi.org/10.1016/j.celrep.2021.109025
26. Uyar B, Palmer D, Kowald A, Murua Escobar H, Barrantes I, Möller S, Akalin A, Fuellen G (2020) Single-cell analyses of aging, inflammation and senescence.Ageing Res Rev. 64:101156.https://doi.org/10.1016/j.arr.2020.101156
27. Miwa S, Kashyap S, Chini E, von Zglinicki T (2022) Mitochondrial dysfunction in cell senescence and aging. J Clin Invest. 132(13).https://doi.org/10.1172/JCI158447
28. Pitceathly RD, Taanman JW, Rahman S, Meunier B, Sadowski M, Cirak S, et al (2013) Cox10 mutations resulting in complex multisystem mitochondrial disease that remains stable into adulthood. JAMA Neurol. 70(12):1556-1561.https://doi.org/10.1001/jamaneurol.2013.3242
29. Hake LE, Kuemmerle N, Hecht NB, Kozak CA (1994) The genes encoding the somatic and testis-specific isotypes of the mouse cytochrome c genes map to paralogous regions of chromosomes 6 and 2. Genomics. 20(3):503-505. https://doi.org/10.1006/geno.1994.1210
30. Zhu W, Jiang H, Xie S, et al (2021) Downregulation of PPA2 expression correlates with poor prognosis of kidney renal clear cell carcinoma. PeerJ. 9:e12086. https://doi.org/10.7717/peerj.12086
31. Ku AF, Sharma KL, Ta HM, et al. Reversible male contraception by targeted inhibition of serine/threonine kinase 33. Science. 2024;384(6698):885-890. https://doi.org/10.1126/science.adl2688

32. Brauksiepe B, Baumgarten L, Reuss S, Schmidt ER (2014) Co-localization of serine/threonine kinase 33 (stk33) and vimentin in the hypothalamus. Cell Tissue Res. 355(1):189-199. https://doi.org/10.1007/s00441-013-1721-8

33. Higo H, Ohashi K, Tomida S, Okawa S, Yamamoto H, Sugimoto S,et al (2022) Identification of targetable kinases in idiopathic pulmonary fibrosis. Respir Res. 23(1):20.https://doi.org/10.1186/s12931-022-01940-y

34. Kanehisa M, Furumichi M, Sato Y, Matsuura Y, Ishiguro-Watanabe M. KEGG: biological systems database as a model of the real world. Nucleic Acids Res. 2025;53(D1):D672-D677. doi:10.1093/nar/gkae909

Figures

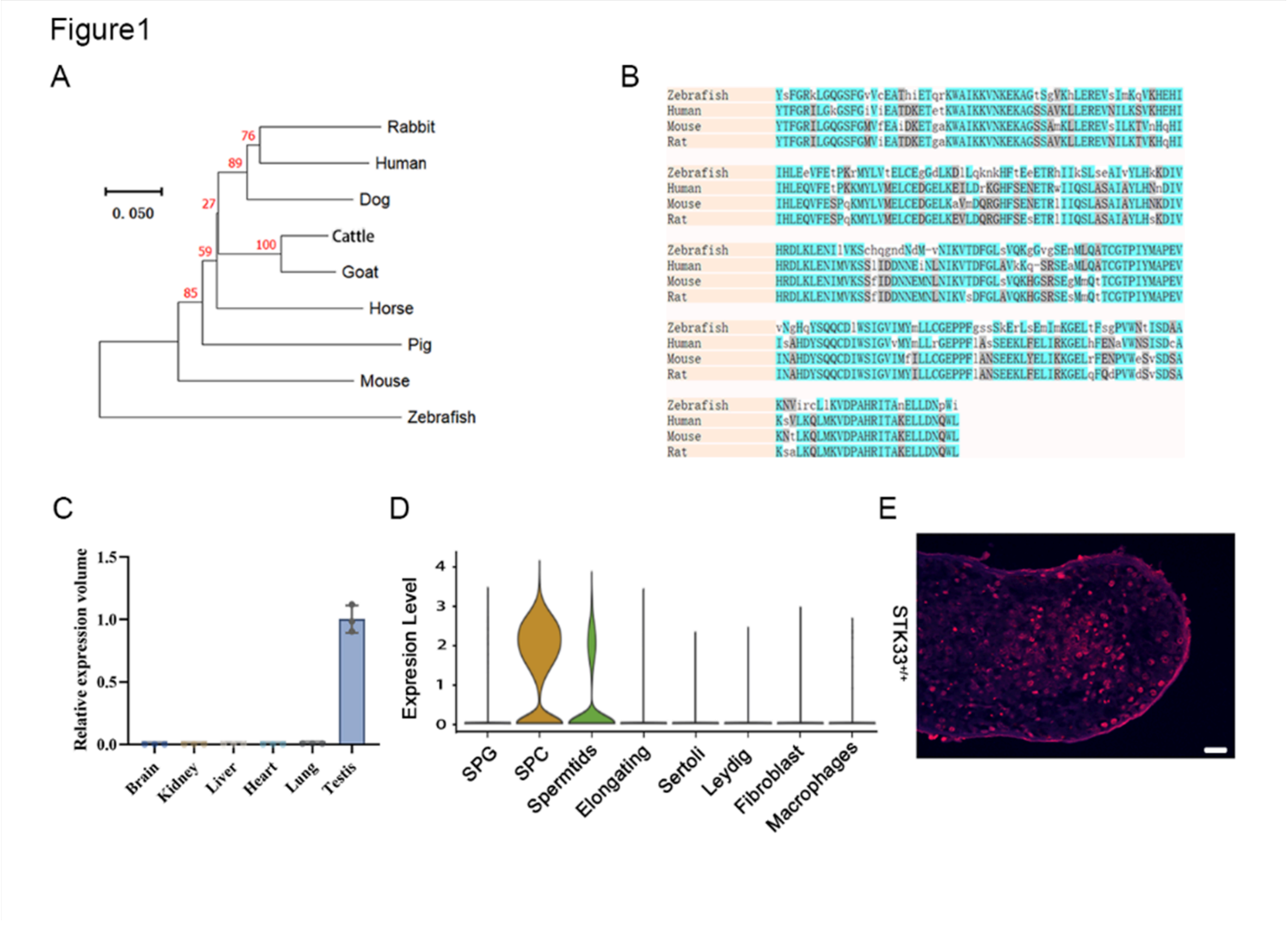


Figure 1

STK33 is specifically expressed in certain stages of germ cells in the testes. A Evolutionary tree analysis of STK33. **B** Sequence alignment of STK33 kinase between common species. **C** RT-PCR result**:**The expression of *STK33* in different tissues from WT 12-week-old C57BL/6 mice. **D** Single-cell

sequencing results: Expression levels of STK33 in different types of testicular cells. SPG: spermatogonial stem cells; SPC: spermatocytes. **E** Immunofuorescent staining of human testicular slices of STK33. Red fluorescence is STK33; blue fuorescence marks the nucleus of DAPI.Scale bars: 50 μm.

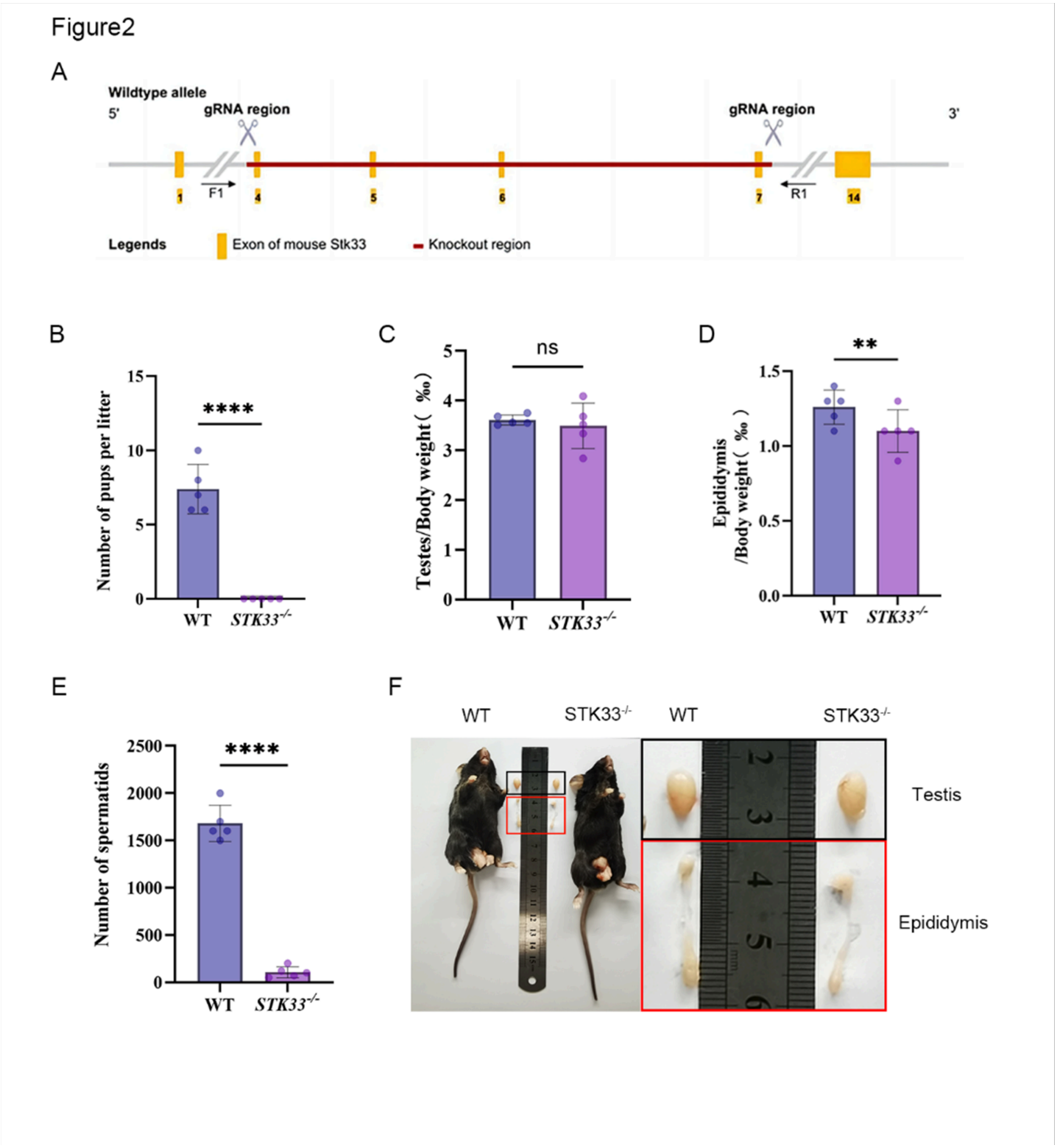


Figure 2

***STK33* deletion leads to male infertility in mice. A** Schematic diagram of *STK33*$^{-/-}$ mice generated by using CRISPR/Cas9 technology. **B** Number of pups per litter from male mice (>8-weeks old) naturally crossed with WT female mice (>6-weeks old) for 6 months. *STK33*$^{-/-}$ male mice showed complete sterility. **C** Testis weight to body weight ratio of WT and *STK33*$^{-/-}$ mice at 12- weeks (n = 4). **D** Epididymis weight to body weight ratio of WT and *STK33*$^{-/-}$ mice at 12- weeks (n = 4). **E** Number of sperm in the epididymis of WT and *STK33*$^{-/-}$ mice at 12- weeks (n = 4). **F** Representative images of testis and cauda epididymidis from WT and *STK33*$^{-/-}$ mice.Data are presented as the mean ± SEM. $p < 0.05$ (*), 0.01 (**), or 0.001 (***),$p>0.05$(ns).

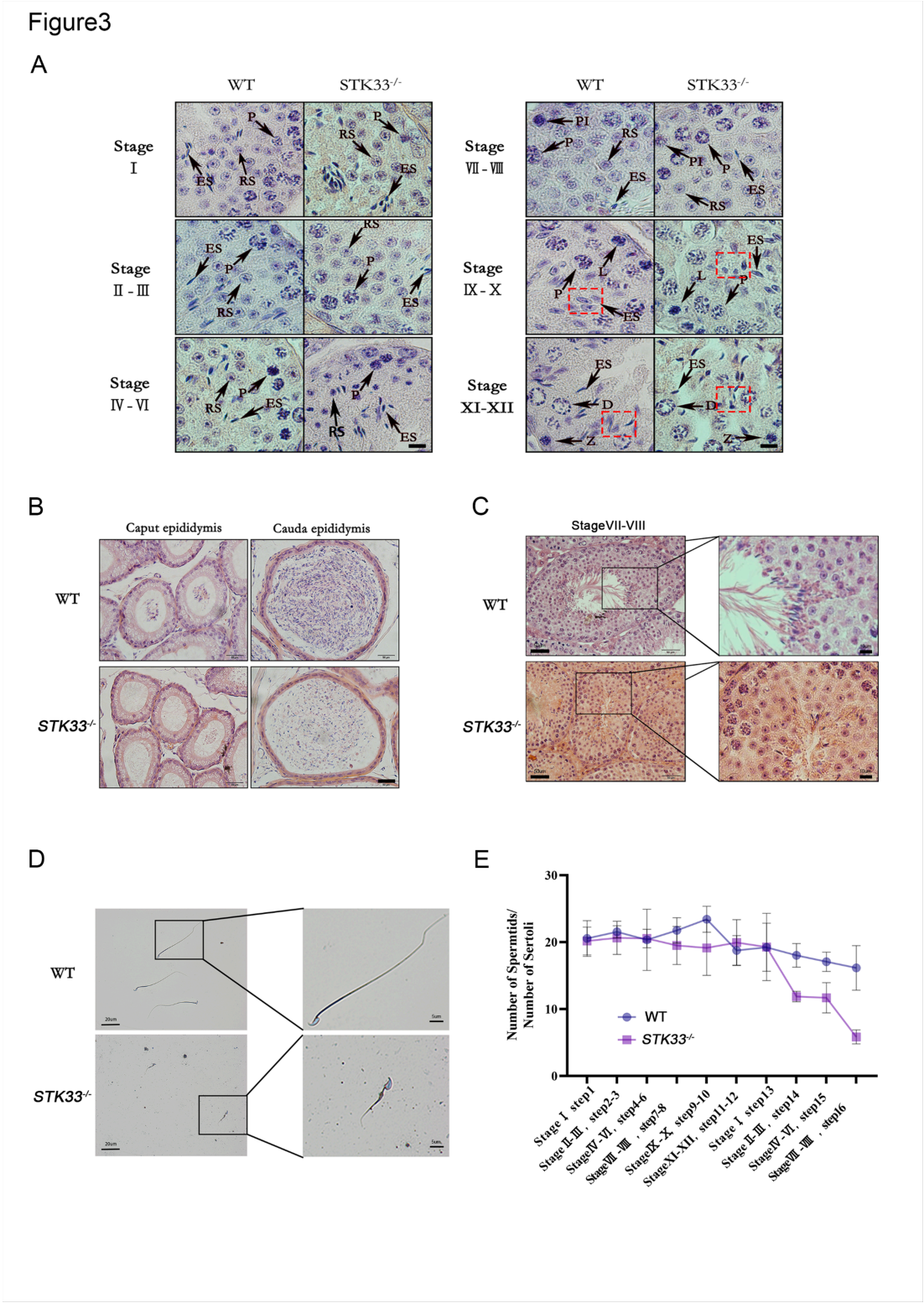


Figure 3

Deletion of the *STK33* leads to a decrease in the quantity of sperm and abnormal morphology. A HE staining of seminiferous tubules from the WT and *STK33*$^{-/-}$ mice. PI:Preleptonema; L:leptotene spermatocytes; Z: zygotene; P: pachytene; D: diplotene; RS:round spermtids; ES:elongating spermtids.Scale bars: 10 μm **B** HE staining of caput and cauda epididymis from the WT and *STK33*$^{-/-}$ mice. Scale bars: 50 μm **C** Diff-quick stain of sperm in epididymis from WT and *STK33*$^{-/-}$ mice. **D** The

number of elongating spermtids in stages VII-VIII. **E** Relative counts of sperm cells at each step in *STK33*$^{-/-}$ mice and WT mice.

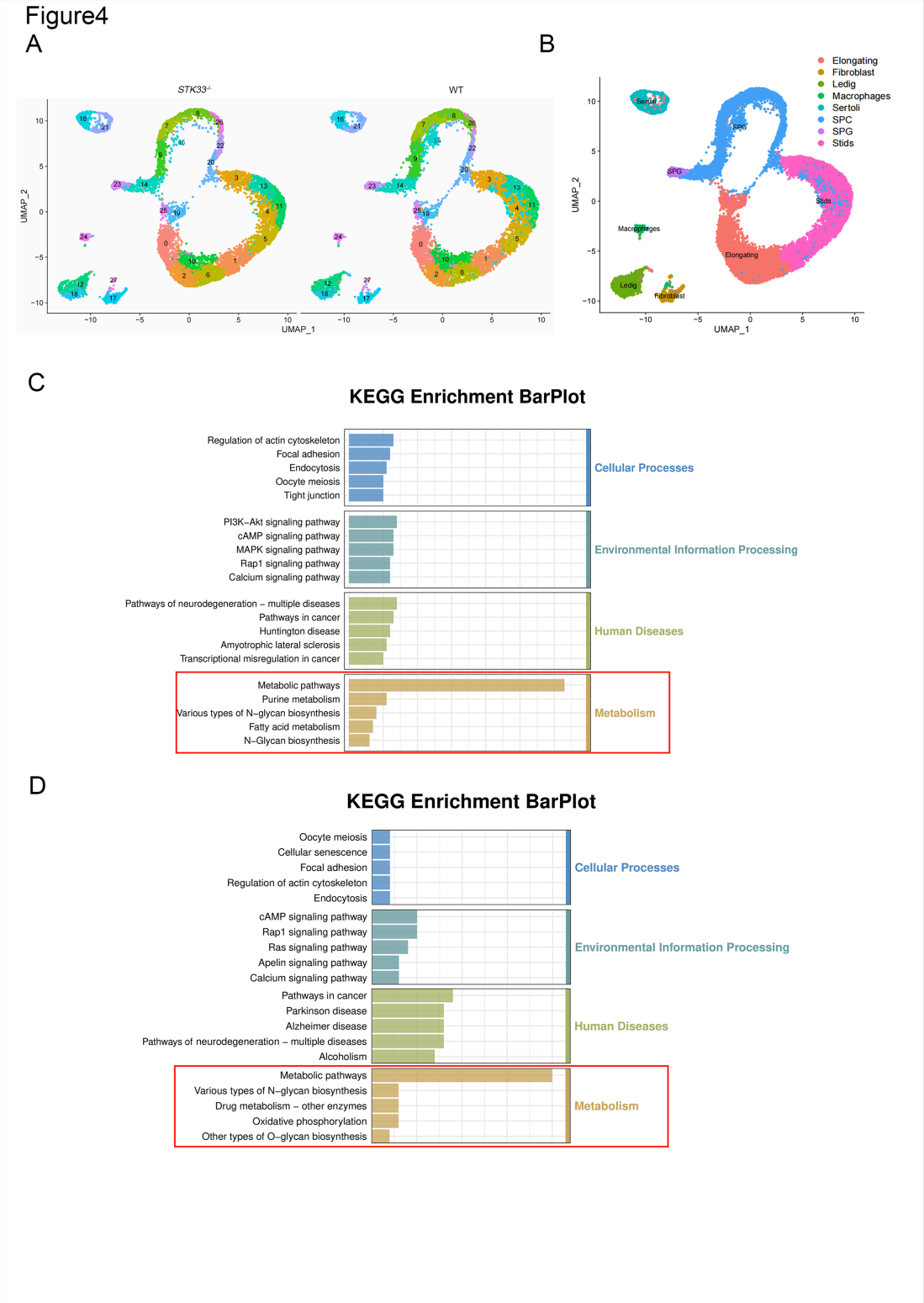


Figure 4

Single-cell sequencing results showed significant abnormalities in the spermatocyte cells of *STK33*$^{-/-}$ mice. A Single-cell sequencing cell subpopulation classification UMAP plots of WT and *STK33*$^{-/-}$ 12-

week-old mice.UMAP, uniform manifold approximation and projection**. B** UMAP plots of WT mice. Cells are colored for types. **C** Differential gene KEGG enrichment pathways of SPC. **D** Differential gene KEGG enrichment pathways of spermtids.

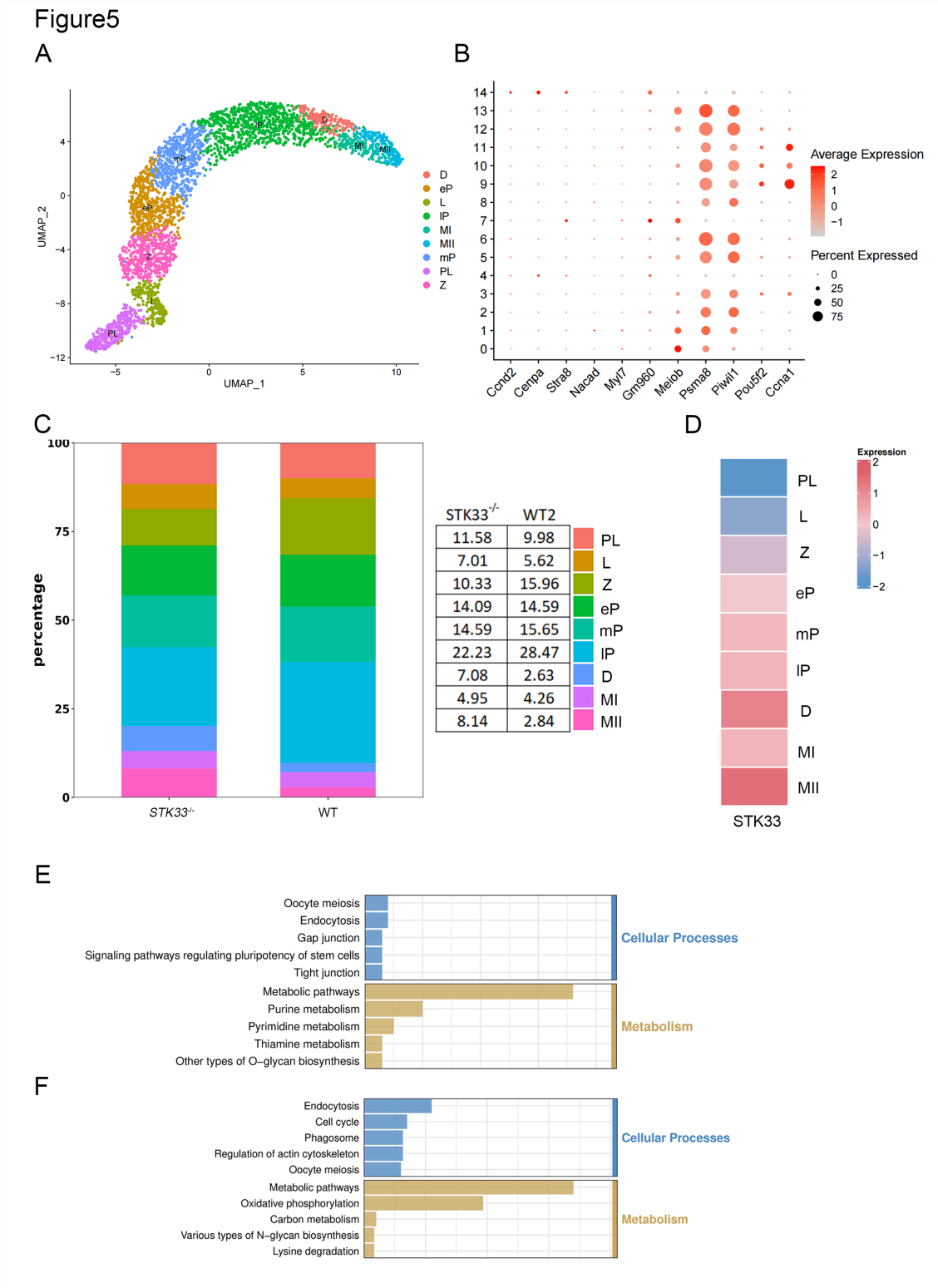


Figure 5

The single-cell sequencing results of SPC subtypes show that the differences between *STK33*$^{-/-}$ and WT are concentrated in metabolic pathways. A Subclassification of SPC UMAP plot. PI:Preleptonema; L:leptotene spermatocytes; Z: zygotene; eP: early pachytene; mP: mid-pachytene; lP: late pachytene; D: diplotene; MI: meiosis I; MII: meiosis II. **B** Heatmap of the expression of maker genes in different SPC clsters. **C** The cell ratio of different subtypes of SPC. **D** Expression heatmap of STK33 in various subcategories of SPC. **E** Differential gene KEGG enrichment pathways of late pachytene SPC clusters. **F** Differential gene KEGG enrichment pathways of zygotene SPC clusters.

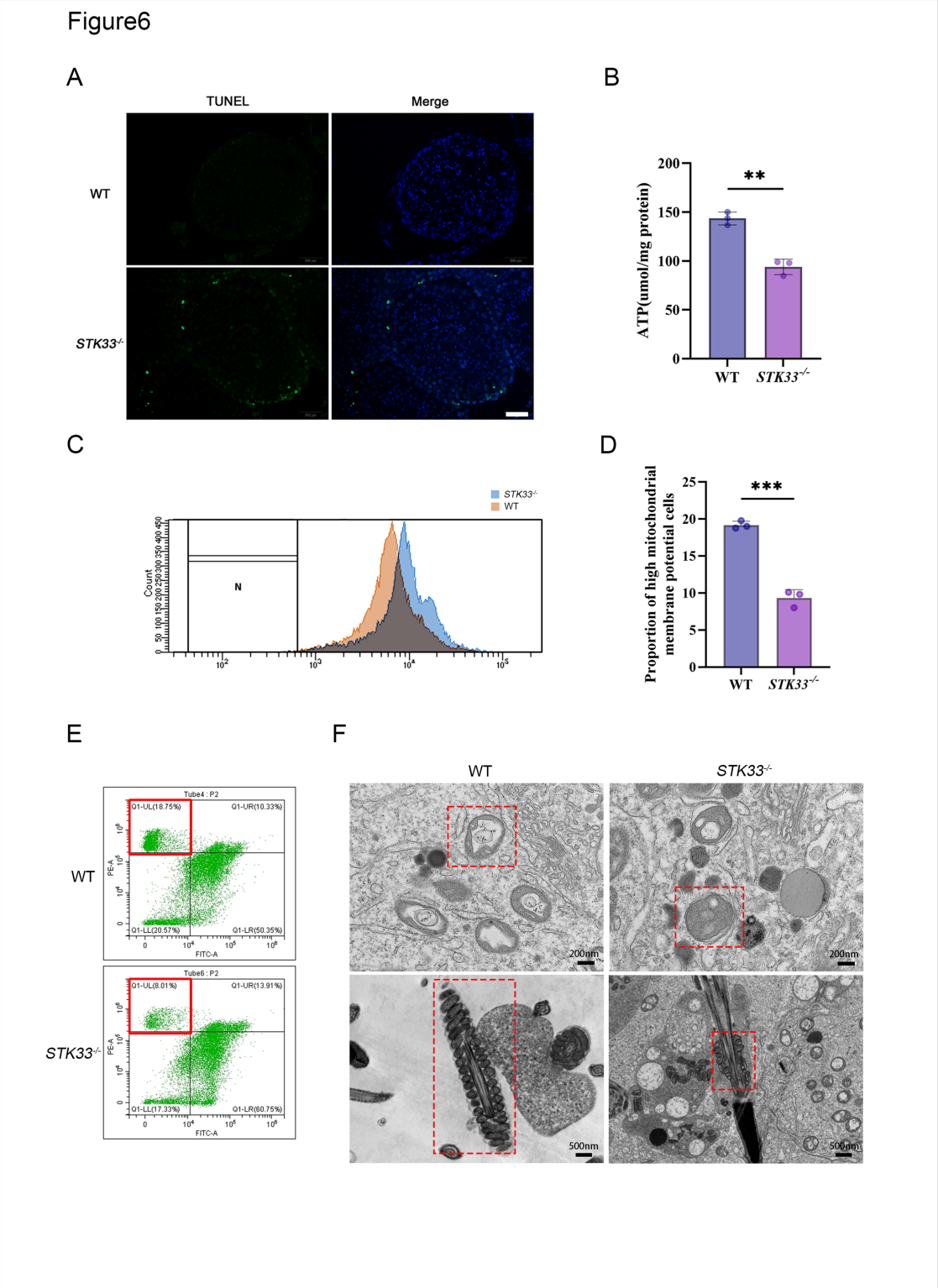


Figure 6

***STK33*$^{-/-}$ mice exhibit increased apoptosis of germ cells and accompanying mitochondrial metabolic abnormalities compared to WT mice. A** TUNEL staining of seminiferous tubules in WT and *STK33*$^{-/-}$ mice testes.Scale bars: 50 μm **B** ATP content in the testicular lysates of WT and *STK33*$^{-/-}$ mice. **C** Comparison of reactive oxygen species(ROS) in spermatogenic cells of WT and *STK33*$^{-/-}$ mice measured by flow cytometry. **D** Results of mitochondrial membrane potential(JC-1) in spermatogenic cells of WT and *STK33*$^{-/-}$ mice determined by flow cytometry. **E** Proportion of cells with high mitochondrial membrane potential in *STK33*$^{-/-}$ and WT mouse testes. **F** Scanning electron microscopy images of mitochondrial morphology and arrangement in the testes of WT and *STK33*$^{-/-}$ mice,mitochondria are indicated by the red box.Data are presented as the mean ± SEM. $p < 0.05$ (*), 0.01 (**), or 0.001 (***),$p>0.05$(ns).

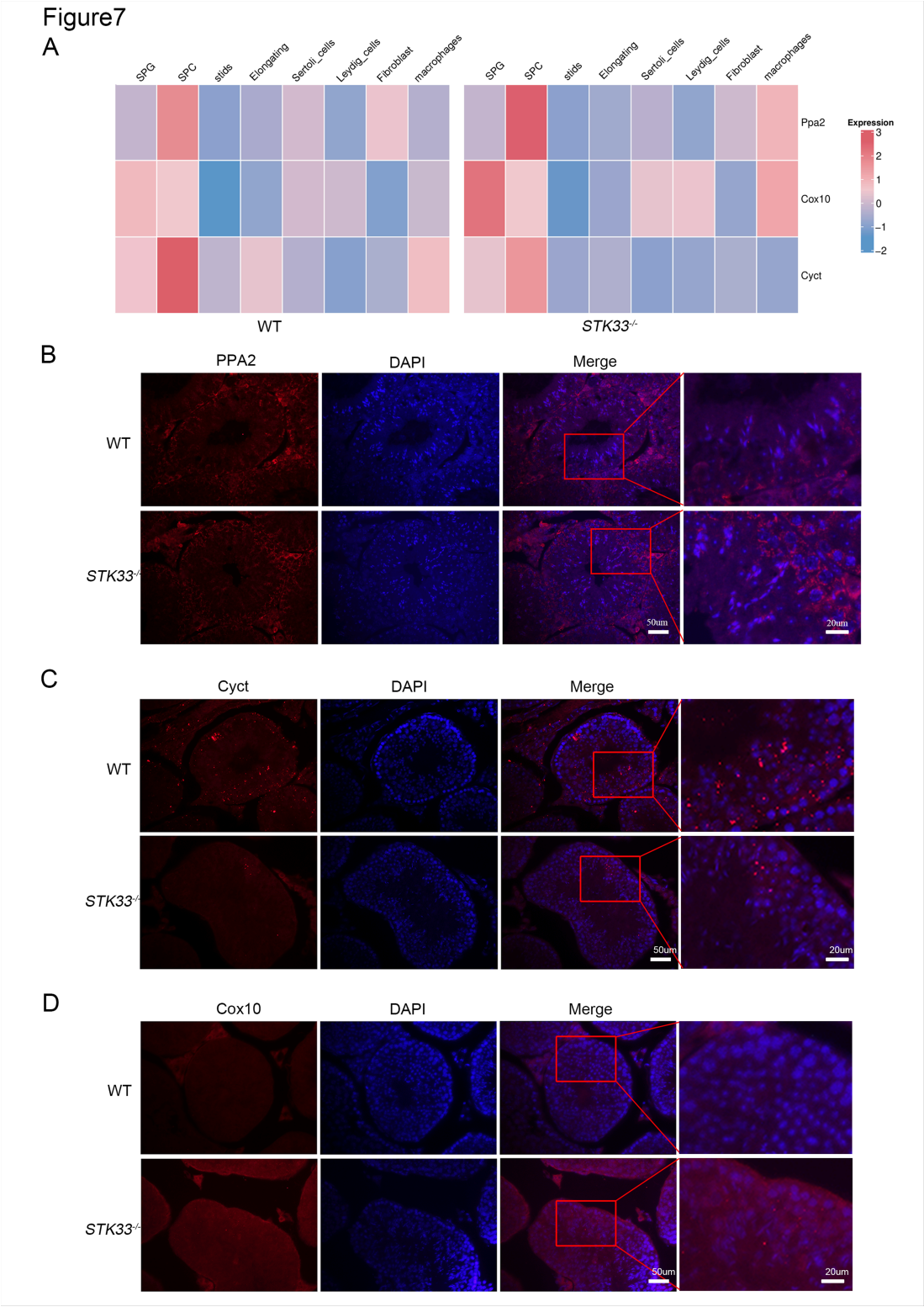


Figure 7

Comparison of differentially expressed genes in the testes of WT and *STK33*$^{-/-}$ mice using single-cell sequencing. A Heatmap of genes' expression in different cell types. **B** Immunofluorescence staining of Ppa2 in the testes of *STK33*$^{-/-}$ and wild-type mice. **C** RNA FISH targeting Cyct was performed for in situ

hybridization in the testes of *STK33*$^{-/-}$ and wild-type mice. **D** RNA FISH targeting Cox10 was performed for in situ hybridization in the testes of *STK33*$^{-/-}$ and wild-type mice.

Supplementary Files

This is a list of supplementary files associated with this preprint. Click to download.

- SupplementaryFigure1.tif
- SupplementaryFigure2.tif
- SupplementaryFigure3.tif
- SupplementaryFigure4.tif